INVITED REVIEW

Recent progress on the planar Hall effect in quantum materials

Jingyuan Zhong(钟景元)[1], Jincheng Zhuang(庄金呈)[1,2,†], and Yi Du(杜轶)[1,2,‡]

[1] *School of Physics, Beihang University, Beijing* 100191, *China*

[2] *Centre of Quantum and Matter Sciences, International Research Institute for Multidisciplinary Science, Beihang University, Beijing* 100191, *China*

(Received 19 December 2022; revised manuscript received 29 January 2023; accepted manuscript online 6 February 2023)

The planar Hall effect (PHE), which originates from anisotropic magnetoresistance, presents a qualitative and simple approach to characterize electronic structures of quantum materials by applying an in-plane rotating magnetic field to induce identical oscillations in both longitudinal and transverse resistances. In this review, we focus on the recent research on the PHE in various quantum materials, including ferromagnetic materials, topological insulators, Weyl semimetals, and orbital anisotropic matters. Firstly, we briefly introduce the family of Hall effect and give a basic deduction of PHE formula with the second-order resistance tensor, showing the mechanism of the characteristic π-period oscillation in trigonometric function form with a $\pi/4$ phase delay between the longitudinal and transverse resistances. Then, we will introduce the four main mechanisms to realize PHE in quantum materials. After that, the origin of the anomalous planar Hall effect (APHE) results, of which the curve shapes deviate from that of PHE, will be reviewed and discussed. Finally, the challenges and prospects for this field of study are discussed.

Keywords: anisotropy, magnetoresistance, planar Hall effect

PACS: 75.47.–m, 73.43.Qt, 85.75.Nn, 75.30.Gw **DOI:** 10.1088/1674-1056/acb91a

1. Introduction

In condensed matter physics, particles are subjected to a periodic potential field and specific boundary conditions to exhibit interesting excitation behaviors, which could be regarded as the counterpart of high-energy physics particles such as Dirac fermions and Weyl fermions.[1–8] The investigation and modulation of these excitation behaviors are of particular interest due to their potential applications. Usually, by applying the external perturbation, the excitation behavior could be drastically modulated. For example, an out-of-plane magnetic field would bring transverse velocity to longitudinal moving electrons in the two-dimensional (2D) electronic system, forming the series of discrete bounding states called Landau level.[9–11] The Landau level evolves into Landau band with energy dispersion along the magnetic field direction in the three-dimensional (3D) system due to the extra space freedom of electrons. The well-known Landau level and Landau band are direct manifestations of magnetic field induced electronic circular motion, generating a number of fascinating Hall effects with the strong correlation to the underlying physics in different matters.[12–15]

For the most studied Hall effect measurements, the magnetic field is applied perpendicular to the current and the plane attached by Hall electrodes. The magnetic field leads to the accumulation of charges along the transverse direction of the current, where the Hall resistance provides the information on the charge carrier density and mobility.[16,17] An intrinsic magnetic moment in the magnetic materials can give rise to a Hall signal deviating from linear behavior due to the interplay of the magnetic moment and external magnetic field, i.e., anomalous Hall effect.[18–20] Furthermore, the spin–orbit coupling (SOC) strength plays the crucial role in the (inverse) spin Hall effect, resulting in the accumulation of spin polarization in the transverse direction.[21–23] For the planar Hall effect (PHE), the direction of the external magnetic field is in the plane attached by Hall electrodes, which is distinct to the above mentioned Hall effects. In general, PHE results from the anisotropic magnetoresistance (AMR) parallel with and perpendicular to the in-plane rotational magnetic field (B) by the measurements of the longitudinal and transverse resistances (R_{xx} and $R_{yx}^{\rm PHE}$). The origin of PHE could be correlated to the intrinsic magnetism, topological property, and anisotropic Fermi surface, providing an effective method to explore and to identify the potential physics in different quantum materials.[24,25,46] There are two specific features for PHE: the first one is the π-period oscillation with the shape of trigonometric function of the angle between B and the applied current; the second one is the 45° phase (φ) difference between R_{xx} curve and $R_{yx}^{\rm PHE}$ curve. Strikingly, some PHE measurements exhibit distorted signal from trigonometric function, which may be the reflection of the correction of weak antilocalization, current jetting effect, anisotropic orbital magnetoresistance, and other complex magnetisms.[40–46] In this review, we call these distorted behaviors as anomalous planar Hall effect (APHE). Recent research indicates that APHE measurement could give a rather

†Corresponding author. E-mail: jincheng@buaa.edu.cn

‡Corresponding author. E-mail: yi_du@buaa.edu.cn

© 2023 Chinese Physical Society and IOP Publishing Ltd

simple method to obtain spin texture information and crystal symmetry of quantum materials.[40,44–46] Therefore, as a special member in Hall family, PHE possesses tremendous potential applications to identify or to confirm the fascinating properties in quantum materials.

In this review, we begin with introducing the family of Hall effect and the origin of PHE in Section 2. In Section 3, we summarize the experimental progress of PHE in ferromagnetic materials, which are caused by coupling between magnetic moment (M) and B. In Section 4, the PHE originated from topological nontrivial band structure is discussed. The spin–momentum locking effect induced backscattering forbidden and chiral anomaly between Weyl nodes provide PHE signal in the surface of topological insulators and Weyl semimetals, respectively. In Section 5, we introduce the mechanism of orbital magnetoresistance which is generated by anisotropic Fermi surface in the presence of in-plane sweeping magnetic field. In Section 6, the distorted PHE with possible explanations is discussed. The origins of some kinds of APHE are still remain mysterious. At the last part, we give a brief summarization of this review and the outlook in this field.

2. Family of Hall effect

Hall effect, as one of most basic measurements of carrier density and mobility, was firstly proposed in 1879 by Edwin Hall to describe the transverse voltage difference in a solid material with an applied longitudinal electric current and an out-of-plane magnetic field. As shown in Fig. 1(a), the charge carriers accumulate along the transverse sides by Lorentz force to provide the electric field force hindering the transverse motion of the following charge carriers. The ideal R_{yx} would show a linear relationship towards the magnetic field, with the slope $k \propto 1/n$, where n is the carrier density, and the sign of the slope represents the type of dominant carriers.[47–49] In an ideal 2D system, the discrete Landau level under the magnetic field emerges to cause perfect quantization resistance platform in R_{yx}, resulting in the integer or fractional quantum Hall effect.[14,50] Significantly, the perfect quantization in R_{yx} implies the discrete feature of quantum mechanism, which sheds light on studying the topology and geometric phase (Berry phase) in condensed matter physics. Some ferromagnetic materials with intrinsic magnetic moment can achieve anomalous Hall effect without applying magnetic field, as shown in Fig. 1(b). Furthermore, 2D clean system with out-of-plane ferromagnetism can achieve zero-field quantized platform, which is classified as quantum anomalous Hall effect. The first experimental realization of quantum anomalous Hall effect was conducted in ultra-high-quality Cr doped topological insulator thin film, showing perfect quantization without external magnetic field at 30 mK.[19] The spin of electrons can also accumulate at edges of samples as shown in Fig. 1(c). The charge current in a system with strong SOC adds different lateral velocities to carriers depending on their spin orientation due to the imbalance of spin-up and spin-down electrons, as shown in Fig. 1(d).[21,23] The electrons residing in 1D spin–momentum locked states in the topological boundary states of 2D topological insulators can be considered as a counterpart of spin Hall effect in quantum regime (zero net charge current).[2,15]

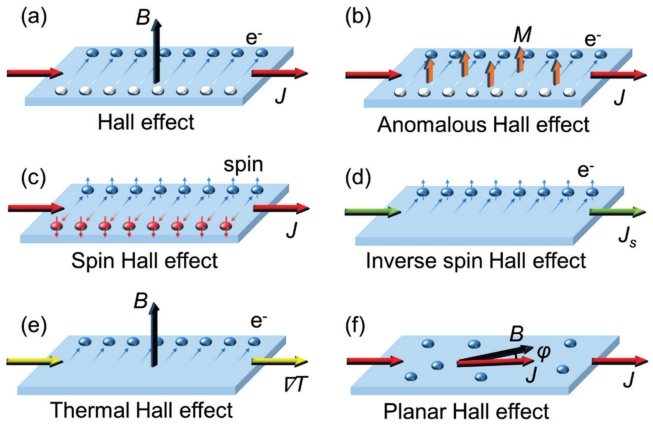


Fig. 1. (a) Schematic of ordinary Hall effect, where the black and red arrows indicate magnetic field B and current density J. The blue balls and white balls represent electrons and holes, respectively. (b) Schematic of anomalous Hall effect, where the orange arrows indicate magnetic moment M. (c) Schematic of spin Hall effect with the spin-up and spin-down electrons separated by SOC to accumulate at opposite side, where the net current perpendicular to J is zero. (d) Schematic of inverse spin Hall effect with an injected spin current density J_s represented by the green arrow. The net current perpendicular to J_s is nonzero because of the inequality of spin-up and spin-down electrons. (e) Schematic of thermal Hall effect with a temperature gradient ∇T shown by the yellow arrow. An out-of-plane magnetic field drifts the electrons perpendicular to ∇T. (f) Schematic of PHE, with φ defined as the angle between in-plane magnetic field and applied electric field (current density). The anisotropic scattering of electrons is manifested in both directions parallel with and perpendicular to the current density.

In heat transport regime, thermal Hall effect exhibits similar behavior as electric Hall effect, as displayed in Fig. 1(e), where the carriers diffusion is evoked by the temperature gradient instead of bias voltage. More specifically, the temperature gradient induces different electron–phonon coupling strength along the direction, evoking carriers group velocity between the hot end and the cold end.[51,52] The trajectory of electrons is bent under the out-of-plane magnetic field, resulting in the accumulation of transverse voltage. If the system possesses intrinsic ferromagnetism, transverse voltage difference can be observed at zero external magnetic field, namely, anomalous Nernst effect.[53,54] Noticing that the electric current may induce heat difference by Joule heat which leads to the Nernst effect, and heat difference may also induce voltage difference to generate electric current. Therefore, the thermal Hall effect and electric Hall effect usually coexist with the variation of intensity.

The schematic of PHE measurement is shown in Fig. 1(f), where φ is defined as the angle between magnetic field and electric current. The anisotropy of the system gives different

response of scattering process, causing the variation of resistance towards different directions, i.e., $R_{\parallel} \neq R_{\perp}$, where $R_{\parallel}$ and $R_{\perp}$ are the resistances parallel with and perpendicular to the magnetic field, respectively. For the measurement coordinate is correlated to the electric current (i.e., the resistances parallel with and perpendicular to electric current, R_{xx} and $R_{yx}^{\rm PHE}$), transformation of the coordinate correlated to magnetic field needs to be conducted. The second-order resistance tensor is convenient to describe the transformation, a 2D system with magnetic field along x direction could be described as[24,25,46]

$$\begin{pmatrix} E_x' \\ E_y' \end{pmatrix} = \begin{pmatrix} R_{\parallel} & 0 \\ 0 & R_{\perp} \end{pmatrix} \begin{pmatrix} J_x' \\ J_y' \end{pmatrix}, \tag{1}$$

where E_x' and E_y' are the electric fields along x and y directions, respectively, and the J_x' and J_y' are the current densities along x and y directions, respectively. Due to the zero off-diagonal elements, it is reasonable to convert Eq. (1) into conductance expression by inversing the resistance matrix (inverse each diagonal element)

$$\begin{pmatrix} J_x' \\ J_y' \end{pmatrix} = \begin{pmatrix} R_{\parallel} & 0 \\ 0 & R_{\perp} \end{pmatrix}^{-1} \begin{pmatrix} E_x' \\ E_y' \end{pmatrix} = \begin{pmatrix} R_{\parallel}^{-1} & 0 \\ 0 & R_{\perp}^{-1} \end{pmatrix} \begin{pmatrix} E_x' \\ E_y' \end{pmatrix} = \begin{pmatrix} G_{\parallel} & 0 \\ 0 & G_{\perp} \end{pmatrix} \begin{pmatrix} E_x' \\ E_y' \end{pmatrix}, \tag{2}$$

where $G_{\parallel}$ and $G_{\perp}$ represent the conductances along x and y directions, respectively. Generally, the resistance expression is used to describe PHE, so here we adopt Eq. (1) for further discussion. Once the in-plane magnetic field rotates after the angle φ, 2D rotation matrix $\boldsymbol{T}$ needs to be introduced,

$$\boldsymbol{T} \begin{pmatrix} E_x' \\ E_y' \end{pmatrix} = \boldsymbol{T} \begin{pmatrix} R_{\parallel} & 0 \\ 0 & R_{\perp} \end{pmatrix} \boldsymbol{T}^{\dagger} \boldsymbol{T} \begin{pmatrix} J_x' \\ J_y' \end{pmatrix}, \tag{3}$$

$$\boldsymbol{T} = \begin{pmatrix} \cos\varphi & -\sin\varphi \\ \sin\varphi & \cos\varphi \end{pmatrix}, \tag{4}$$

where $\boldsymbol{T}$ transforms the magnetic field relevant coordinate to the electric current relevant coordinate. After applying this transformation, Eq. (3) could be written as

$$\begin{pmatrix} E_x \\ E_y \end{pmatrix} = \begin{pmatrix} \cos\varphi & -\sin\varphi \\ \sin\varphi & \cos\varphi \end{pmatrix} \begin{pmatrix} R_{\parallel} & 0 \\ 0 & R_{\perp} \end{pmatrix} \begin{pmatrix} \cos\varphi & \sin\varphi \\ -\sin\varphi & \cos\varphi \end{pmatrix} \begin{pmatrix} J_x \\ J_y \end{pmatrix} = \begin{pmatrix} R_{\perp} + (R_{\parallel} - R_{\perp})\cos 2\varphi & (R_{\parallel} - R_{\perp})\sin\varphi\cos\varphi \\ (R_{\parallel} - R_{\perp})\sin\varphi\cos\varphi & R_{\perp} + (R_{\parallel} - R_{\perp})\sin 2\varphi \end{pmatrix}. \tag{5}$$

If we define the current direction along x axis, $J_y = 0$ and the final expression of PHE could be obtained as

$$R_{xx} = R_{\perp} + (R_{\parallel} - R_{\perp})\cos^2\varphi, \tag{6}$$

$$R_{yx}^{\rm PHE} = (R_{\parallel} - R_{\perp})\sin\varphi\cos\varphi. \tag{7}$$

According to Eqs. (6) and (7), the two key characteristics of PHE, trigonometric function oscillation and the 45° phase difference, can be clearly implied. The anisotropy of the system ($\Delta R = R_{\parallel} - R_{\perp}$) under the magnetic field determines the amplitude of PHE oscillation. In a perfect isotropic 2D system, the amplitude equals to zero, leading to the disappearance of PHE. While in a strong anisotropic 2D system, the amplitude is large, leading to extensive PHE. It should be noted that the field-dependent measurement of PHE would provide symmetric signal towards B, contradicting to the ordinary Hall effect which is antisymmetric towards B. The origin of PHE amplitude may be complicated, and different quantum materials may possess diverse mechanisms to provide the anisotropy.

The misalignment of magnetic field and electrodes can evoke immense deviation from theoretical predictions. Usually, the misalignment of magnetic field and electrodes would generate ordinary Hall effect signal ($R_{yx}^{\rm OHE}$) and the longitudinal AMR signal (R_{xx}), respectively. Therefore, the measured transverse resistance can be expressed as

$$R_{yx} = R_{yx}^{\rm PHE} + R_{yx}^{\rm OHE} + R_{xx}. \tag{8}$$

The above three terms have different period or symmetry towards angle φ. Firstly, $R_{yx}^{\rm PHE}$ and $R_{yx}^{\rm OHE}$ are antisymmetric towards φ, but R_{xx} is symmetric towards φ. The overall transverse resistance can be divided into two parts

$$R_{yx}' = R_{yx}^{\rm PHE} + R_{yx}^{\rm OHE} = (R_{yx}(\varphi) - R_{yx}(-\varphi))/2, \tag{9}$$

$$R_{xx} = (R_{yx}(\varphi) + R_{yx}(-\varphi))/2. \tag{10}$$

Then, $R_{yx}^{\rm PHE}$ and $R_{yx}^{\rm OHE}$ can be separated by the period difference, where the former is π-period but the latter is 2π-period. This process can be expressed by

$$R_{yx}^{\rm PHE} = (R_{yx}'(\varphi) + R_{yx}'(\varphi + \pi))/2, \tag{11}$$

$$R_{yx}^{\rm OHE} = (R_{yx}'(\varphi) - R_{yx}'(\varphi + \pi))/2. \tag{12}$$

As for the field-dependent measurement, similar process can be conducted to obtain $R_{yx}^{\rm PHE}$ (strictly symmetric signal towards B). Thus, the influence of misalignments on the measured results can be effectively eliminated. After figuring out the basic mechanisms of PHE measurement, we next discuss the origin of anisotropy in the quantum materials.

3. PHE in ferromagnetic materials

Theoretically, the thin films made up by 3d ferromagnetic elements, such as Fe, Co, Ni, are predicted to show PHE due to their in-plane magnetization.[55–57] In experiments, the

PHE was firstly observed in ferromagnetic materials, such as (Ga,Mn)As, Fe_3O_4, Fe_3Si thin films, where the scattering process of electrons can be largely influenced by spin orientations. The PHE signal can be adjusted by both the intrinsic magnetism and the extrinsic magnetic field.[24–26] In ferromagnetic materials, when temperature is lower than the transition temperature, the spin orientations tend to align unidirectionally. A strong enough external field would alter the direction of spin polarization, inducing an identical PHE behavior as suggested by Eqs. (6) and (7) with an in-plane sweeping magnetic field. When the magnetic field is large enough to saturate the magnetic moment in a sample, the rotation of in-plane magnetic field possesses the identical role of the rotation of in-plane magnetic moment, leading to the observation of ideal PHE (the effective value of B may change due to the function of magnetic moment). However, when the magnetic field is relatively small, the interaction among external field, internal magnetic momentum, and scattering process of carriers can be complex and remained unclear, resulting in the deviated PHE signal from ideal trigonometric function.[25] As shown in Fig. 2(a), with the increase of the magnetic field, the angle-dependent PHE transforms from distorted shape to normal trigonometric function, where the blue solid lines and red dashed lines indicate positive and negative sweeping directions of the magnetic field, respectively. This distortion can be observed even more clearly in field-dependent PHE measurement, as shown in Figs. 2(b) and 2(c), where there are two jumps in each sweeping process. The positions of the first jumps are almost the same but the positions of the second jumps vary with φ, where the two jumps overlap at $\varphi = \pm 30^\circ$. This peculiar phenomenon has been attributed to domain reversal with anisotropic magnetocrystalline energy surface, but still parts of the observations remain mysterious.[25,58] Notice that magnetic system usually shows high conductivity, resulting in the low signal-to-noisy ratio of PHE measurement. The best signal of PHE in magnetic system is reported in ferromagnetic semiconductor (Ga,Mn)As thin film, where the highly resolved PHE is 4 orders higher in intensity than the previous PHE results in metallic magnetic materials.[59,60] In Fe_3O_4 thin films, strong PHE signals have also been observed when temperature is lower than the Verway transition point, although the clear angle-dependent PHE evidence is absent.[26] Interestingly, the Berry phase can also influence PHE in Heusler alloy $Fe_{3+x}Si_{1-x}$, which is attributed to the magnetic interaction with the reduced crystal symmetry.[24] The factors in magnetic system , e.g., magnetic domains and disorder, affect the anisotropy and provide both opportunities and challenges to understand the complex mechanism of magnetic anisotropy. Furthermore, it is proposed that the PHE in magnetic thin films has the potential to build magnetic random-access memory to replace the magnetic tunnel junction.[61,62]

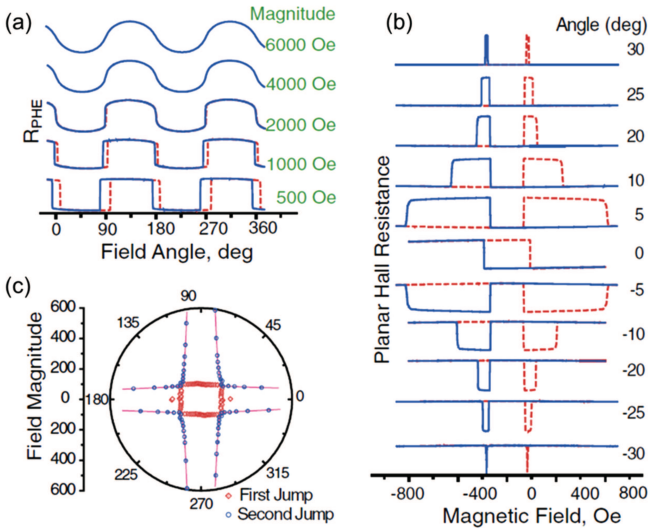


Fig. 2. (a) Angle-dependent PHE measurement under different magnitude of external magnetic field.[25] The blue solid lines and red dashed lines represent the sweeping of positive and negative magnetic fields, respectively. (b) Field-dependent PHE measurement at different φ, where the blue lines and red dashed lines indicate the left sweeping and right sweeping processes, respectively.[25] (c) Polar plot with extracted jumping positions in (b), where at $\varphi = \pm 30^\circ$ the two jumps overlap.[25]

4. PHE in topological non-trivial materials

As one of the quantum materials, topological non-trivial materials have evoked tremendous interests in the condensed matter physics due to their fascinating mechanisms and potential application of spintronics. The unique bulk–boundary correspondence provides novel properties in topological insulators and Dirac/Weyl semimetals, resulting in the topological surface states and Fermi arcs with special spin orientations.[1–8] PHE can be achieved in these materials due to the anisotropy originated from topological surfaces states and chiral anomaly between Weyl nods, providing the transport methods to analyze the topological non-trivial characteristic.

For topological insulators, the strong SOC induces inversion of energy bands, and opens topological non-trivial gap with topological surface states residing in it, as shown in Fig. 3(a). Taking 3D strong topological insulators in Fig. 3(b) as an example, the topological surface states possess the two-fold degenerated Dirac points at each surface (namely, the helical surface states). The topological surface states are occupied by the spin–momentum locked carriers, leading to the prohibition of electrons backscattering.[1,2] The key issue to retain the spin–momentum locking states is the reservation of time-reversal symmetry. Generally, a magnetic field perpendicular to spins would break time-reversal symmetry, lifting the prohibition of electrons backscattering in topological surface states.[27–29] The electrons moving parallel with magnetic field have the spins perpendicular to the magnetic field, causing the time-reversal breaking process and finally increasing

the resistance along this direction. On the contrary, the electrons moving perpendicular to magnetic field may have the spins parallel with the magnetic field, preserving the time-reversal symmetry and keeping the prohibition of backscattering. This process contributes to the increase of the resistance parallel with the magnetic field ($R_{\parallel}$) and the unchanged resistance perpendicular to the magnetic field ($R_{\perp}$) in topological surface states with the in-plane magnetic field, resulting in the anisotropy acquired by PHE ($\Delta R > 0$), as shown in Fig. 3(c).[27] The PHE and AMR results in topological insulator thin film $Bi_{2-x}Sb_xTe_3$ are displayed in Figs. 3(d) and 3(e), respectively, where clear positive amplitude can be observed.[28] The amplitude of PHE originated from topological surface states has different dependence towards the intensity of the magnetic field, which has been identified as quasi-linear or linear tendency.[27,28] As shown in Fig. 3(f), the shape of PHE strictly follows trigonometric function and the amplitude shows a good linear field-dependent behavior at high magnetic field, contradicting with the predicted parabolic field-dependence originated from chiral anomaly and orbital magnetoresistance.[27,32] However, there is a low-field deviation from linear dependence in Fig. 3(f), of which the origin is still unexplained. In another PHE measurement in Sn doped topological insulator $Bi_{1.1}Sb_{0.9}Te_2S$, the PHE amplitude shows better linear relationship towards magnetic field.[28] For the clear observation of PHE in topological surface states, the depletion of the contribution from bulk carriers is required. Figure 3(g) shows the PHE amplitude dependence towards gating voltage to modulate the position of Fermi level relevant to the surface states. The predominant surface states guarantee the positive amplitude under a large range of gating voltage. Notice that the overall PHE amplitude shows two peaks and a minimum near the Dirac point, which is attributed to the influence of randomly distributed disorder in topological insulators.[27]

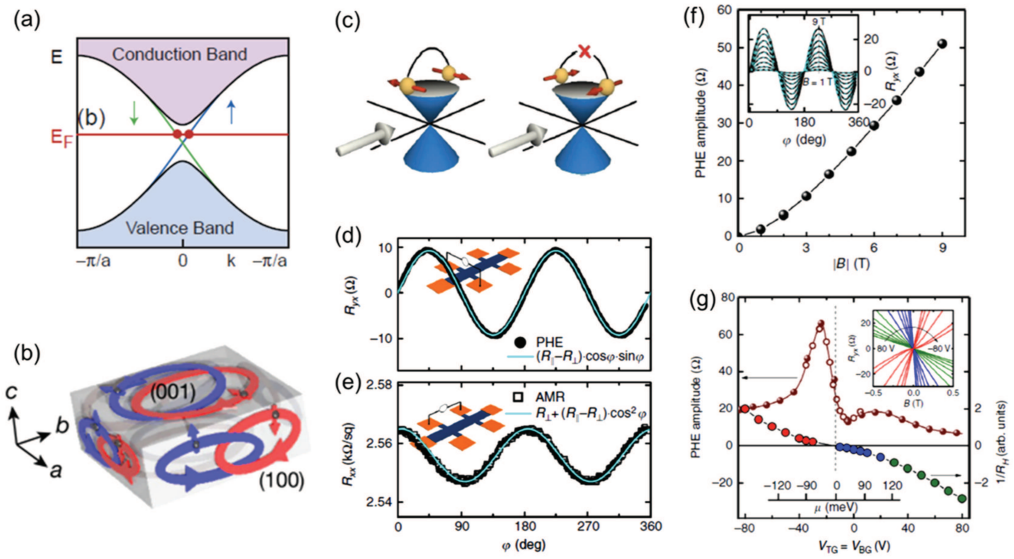


Fig. 3. (a) Schematic of topological surface states (green and blue lines) with green and blue arrows indicating the spins.[1] (b) Schematic of strong topological insulators with helical surface states.[3] (c) Schematic of time-reversal symmetry breaking process by in-plane magnetic field, where the red arrows indicate spins of electrons and the white arrows represent magnetic field.[27] The magnetic field perpendicular to spin direction (left panel) would break time-reversal symmetry, allowing the backscattering of electrons along magnetic field. The parallel magnetic field to spin direction (right panel) reserves time-reversal symmetry, forbidding the backscattering of electrons perpendicular to magnetic field. (d) Angle-dependent PHE and AMR measurement in topological insulator thin film $Bi_{2-x}Sb_xTe_3$.[27] (f) The amplitude of PHE under different strength of magnetic field, where a linear tendency is observed at high magnetic field. The inset shows the angle-dependent PHE curves from $B = 1$ T to 9 T.[27] (g) PHE amplitude (left axis) under different gating voltage, i.e., the Fermi surface is located at different energy, where the dashed line indicates the location of the Dirac point.[27] The right axis shows carrier types transition with gating voltage, confirming that the PHE signal originates from topological surface states rather than bulk states. The inset shows ordinary Hall signal, where the slopes change from positive to negative implies the location of the Dirac point.

On the contrary, if the Fermi surface moves into bulk states with considerable bulk carriers, the orbital magnetoresistance effect may surpass the effect of topological surface states, altering the PHE amplitude from positive to negative. Unavoidably, the impurity or disorder in gapped bulk materials contributes to impurity energy level within the band gap, which may disturb the intrinsic PHE signal. Once the impurity dominates the electric transport behavior, the extra carriers induced by disorder may conceal the intrinsic anisotropic band structure, such as the disorder induced double-peak behavior near the Dirac points in $Bi_{2-x}Sb_xTe_3$.[27] One direct method to deal with this problem is to improve the quality of sample, where the molecular beam epitaxy technique can effectively reduce the disorder. Also, gating voltage is useful to amplify the intrinsic signal by controlling the Fermi level located near the Dirac or Weyl points.

Weyl semimetals, as the product of breaking time-reversal symmetry or inversion symmetry in Dirac semimetals, would

possess even number of Weyl nodes in their gapless bulk band structure.[4–8] PHE observed in Weyl semimetals originates from the charge pumping effect between two Weyl nodes under the external magnetic field.[32] A pair of Weyl nodes with different chirality (+1 or −1) emerges and annihilates simultaneously, corresponding to the annihilation and emergence of a Dirac point, respectively. Each pair Weyl nodes can generate non-trivial Berry phase from one Weyl node (source of Berry curvature) to the other Weyl node (sink of Berry curvature), causing the topologically protected Fermi surface connecting a pair of Weyl nodes and consequently forming the Fermi arc. In the presence of magnetic field, the lowest Landau level at Weyl nodes exhibits opposite linear dispersion with opposite group velocity according to its chirality, as shown in Fig. 4(a). Applying an electric field parallel with the magnetic field would induce the imbalance of chemical potential between two Weyl nodes, which transfers extra electrons from the high potential Weyl node to the low potential Weyl node.

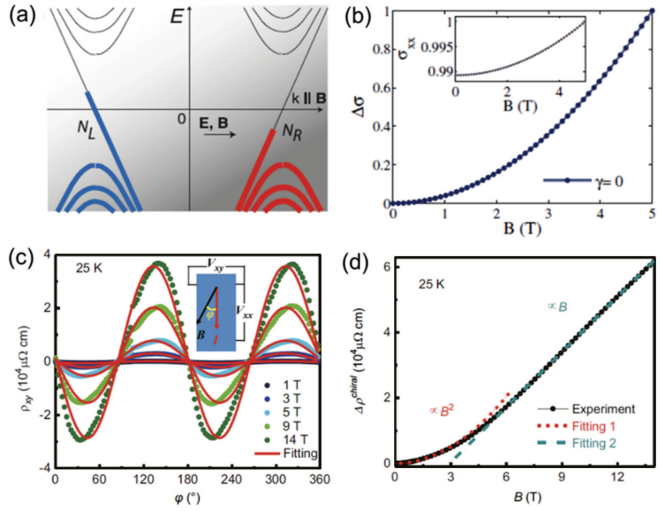


Fig. 4. (a) Schematic of charge pumping between Weyl nodes induced by chiral anomaly, where N_L and N_R represent left-handed and right-handed electrons in Weyl nodes.[64] The magnetic field induces chiral linear lowest Landau level at two Weyl nodes, and the parallel electric field introduces the imbalance of chemical potential (the blue and red lines). (b) Theoretically predicted PHE amplitude in the expression of conductivity and the longitudinal magnetoconductivity (inset), where clear parabolic tendency towards magnetic field is observed.[32] The γ is a tilting parameter, and $\gamma = 0$ represents a type-I Weyl semimetal. (c) Angle-dependent PHE measurement in elemental semiconductor tellurium under different magnetic field.[35] (d) PHE amplitude dependency towards magnetic field, where the low-field behavior shows parabolic relationship, while the high-field behavior shows linear relationship.[35]

Consequently, the applied parallel electric field and magnetic field pump additional electrons along this direction, and the intensity of pumping increases with the increase of the magnetic field, evoking the negative magnetoresistance effect by chiral anomaly.[63,64] Comparing with PHE in topological insulators, the sign of PHE amplitude in Weyl semimetals is negative due to the reduced resistance along the magnetic field ($\Delta R < 0$). The theoretical prediction of PHE amplitude in Weyl semimetals as a function of magnetic field is shown in Fig. 4(b), where the perfect parabolic tendencies in both PHE amplitude and longitudinal conductivity are expected. In experiments, the elemental semiconductor tellurium possesses a pair of Weyl nodes separating along k_y direction, which is supposed to provide negative magnetoresistance when the magnetic field and electric field are both parallel with the crystallographic b axis.[35] Indeed, the PHE results in tellurium agree well with the prediction as shown in Fig. 4(c), despite of the slight deviation from the perfect trigonometric function. The PHE provides an extra manifestation of chiral anomaly in Weyl physics in addition to negative magnetoresistance. There are still some phenomena in PHE which need to be further studied, such as the distortion from perfect trigonometric function and the abnormal field-dependent PHE amplitude in Fig. 4(d).

5. Orbital magnetoresistance and relevant PHE

Besides the above three mechanisms, the most general one to induce PHE is the orbital magnetoresistance effect, which is determined by the shape of Fermi surface. Lorentz force, as the direct effect of magnetic field, gives electrons transverse velocity. The resistance would be enhanced by magnetic field due to the increased possibility of scattering events, namely, orbital magnetoresistance.[65–67] The increase of resistance is strongly correlated to the magnetic field and the mobility of electrons (i.e., the shape of Fermi surface), so an in-plane magnetic field in a system with anisotropic electrons mobility might induce non-zero PHE amplitude, leading to sine or cosine type oscillation in transverse resistance.[36–43] Usually, the electrons with higher mobility would exhibit larger increasement of magnetoresistance. The Fermi surface in bismuth possesses large anisotropy of Fermi surface with three high-symmetric axes called bisectrix, trigonal and binary axes in Brillouin zone of bismuth.[65] Figure 5(a) shows the Fermi surface perpendicular to the trigonal axis, where three highly anisotropic Dirac-type electron pockets are separated around the trigonal axis by an interval angle of 120°, and a hole pocket is located along the trigonal axis. The transverse resistivity as a function of the angle between binary axis and magnetic field is shown in Fig. 5(b), where the six-fold oscillation coincides with the 60° interval angle between two nearest long axe of the ellipsoid electron pockets. In some other materials, the symmetry of Fermi surface may not be perfect three-fold or six-fold, but possess the orbital magnetoresistance difference along two orthogonal directions ($R_{\parallel}$ and $R_{\perp}$), which could also evoke the non-zero PHE amplitude.[36–43] Figures 5(c) and 5(d) show the PHE and longitudinal resistivity measurement in Weyl semimetal $PdTe_2$, respectively, where the origin of PHE is a mixture of orbital magnetoresistance and chiral anomaly.[43] Notice that the amplitude of PHE induced by orbital magnetoresistance is negative, similar to that induced by chiral anomaly, hindering

the identification of the contribution of orbital magnetoresistance from chiral anomaly in Weyl semimetals. The observation of PHE induced by orbital magnetoresistance depends on the value of anisotropy and the resolution of electric transport. In quasi-1D materials, such as high order topological insulator Bi_4Br_4 and topological superconductor $TaSe_3$, clear PHE results induced by anisotropic orbital magnetoresistance have been reported.[40]

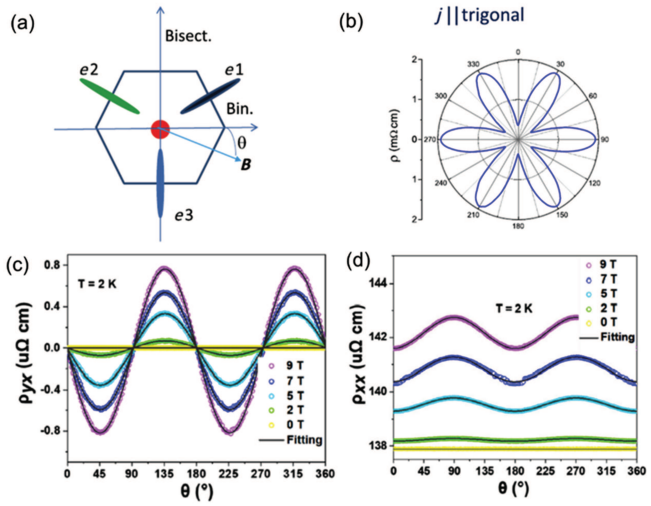


Fig. 5. (a) Schematic of the projected Fermi surface perpendicular to the trigonal axis in bismuth, where the three electron pockets are colored by dark blue, green, light blue, respectively, and the hole pocket is colored by red. The angle between the binary axis and magnetic field is defined as θ.[65] (b) Angle-dependent transverse orbital magnetoresistance under the configuration of (a), where the six-fold symmetry coincides with the location of the three electron pockets.[65] (c) Angle-dependent PHE and (d) longitudinal resistivity in $PdTe_2$ with the form of trigonometric function and negative PHE amplitude.[43]

6. APHE

There are some abnormal PHE results with the curve shape deviating from perfect sine of cosine type, which are attributed to APHE. The APHE results have been reported in various kinds of materials, such as quasi-1D topological insulator Bi_4Br_4, magnetic topological insulator $MnBi_2Te_4$, Weyl semimetal TaP, the (111) oxide interface between $LaAlO_3$ and $SrTiO_3$, and so on.[40,41,45,46] The interpretations of these anomalous behavior are correlated to many factors, such as electronic coherence, orbital magnetic moment, current jetting effect, symmetry information of crystal structure, and so on. Sufficient understanding of these anomalous distortion may generate inspiration towards underlying interaction among electrons, spins, and symmetry of band structure, providing additional means to analyze SOC and anisotropy of Fermi surface in these quantum materials.

High order topological insulator Bi_4Br_4 is made up by the unique quasi-1D molecular chains, which stack along two directions through van der Waals interaction.[68–70] Recently, it was reported that the non-trivial Berry phase in the (100) surface of Bi_4Br_4 leads to weak antilocalization, acting as a low-temperature resistance correction by the coherence behavior between trajectories of the electron and its time-reversal state.[70] Once there is an external magnetic field perpendicular to the trajectory of electrons, the coherent transport vanishes, giving rise to a cusp-like magnetoresistance curve. The highly anisotropic band structure of Bi_4Br_4 makes the coherence behavior mostly occur along the low-resistance direction (along the chain). The in-plane rotating magnetic field would periodically break the weak antilocalization and results in the enhanced slope, as shown schematic in Figs. 6(a) and 6(b). Therefore, the weak antilocalization tends to emerge in the spin-polarized system where the spin orientations are aligned parallel or antiparallel, which can be detected by the distorted behavior in low-temperature APHE.

Beside the electronic coherence induced correction on PHE, the magnetism could induce extra characteristics in low-temperature and high-field PHE measurement. In magnetic topological $MnBi_2Te_4$, the longitudinal resistivity and PHE are shown in Figs. 6(c) and 6(d), where the PHE is evolved to $\pi/2$-period oscillation in trigonometric function form under high magnetic field.[45] The low-field π-period oscillation has positive amplitude but the high-field $\pi/2$-period oscillation has negative amplitude, originating from the surface states and the bulk states, respectively. The in-plane rotating magnetic field generates the parallel orbital magnetic moment and Berry curvature, leading to the positive-amplitude π-period PHE signal from the surface states and both the negative-amplitude π-period and $\pi/2$-period signals from the bulk states.[45,71] Due to the antiferromagnetic ground state of $MnBi_2Te_4$, the surface and bulk PHE currents are antiparallel with each other, canceling the π-period signals and leaving the $\pi/2$-period oscillated PHE at high field. Thus, this APHE originates from the competition between topological surface states and bulk states in the magnetic topological insulator, which may provide further information to judge the origin of dominant carriers.

A classical phenomenon called current jetting effect can also induce corrections on PHE results as observed in Weyl semimetals TaP.[41] When the magnetic field is applied parallel to the electric field, the Lorentz force would constrain electrons circulating around the magnetic field, making the imbalanced current density distribution. The current density is therefore condensed to the interior space of the sample, giving rise to the reduced voltage measured by the electrodes at the edges. Therefore, the overall observation of current jetting is similar to negative magnetoresistance in Weyl semimetals, which is inevitable to happen because the real electrodes have width and can not be perfectly aligned.[64] For the APHE induced by current jetting, it is claimed that the high mobility of electrons results in strong current jetting effect, inducing the enhanced slope and double-peaks curves in the APHE results displayed in Figs. 6(e) and 6(f). However, the theory connecting the current jetting effect and APHE is still missing.

Moreover, the symmetry of crystal structure can also induce APHE, which is similar to the anisotropic orbital magne-

toresistance evoked multi-fold oscillation. For example, the (111) oxide interface between $LaAlO_3$ and $SrTiO_3$ exhibits distorted PHE, as shown in Fig. 6(g).[46] The distortion could be tuned by gating voltage, indicating that the location of Fermi surface is crucial in the observation of APHE. There are two-fold, four-fold and six-fold oscillation signals extracted from the distorted PHE, corresponding to the symmetry of the atomic configuration.

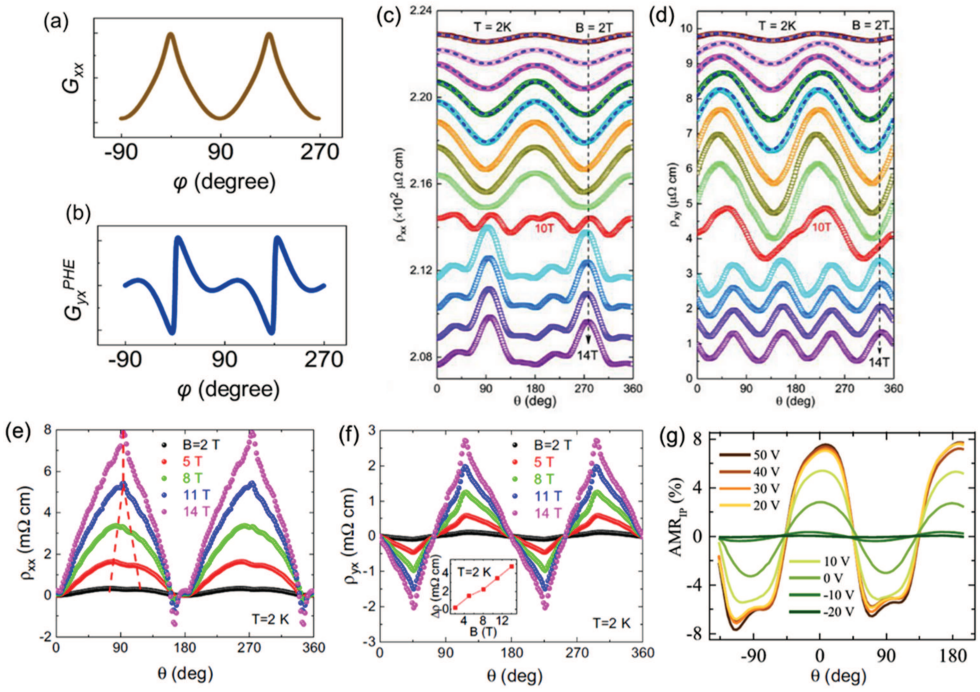


Fig. 6. (a) Schematic angle-dependent longitudinal conductance and (b) corresponding APHE in quasi-1D topological insulator Bi_4Br_4, where the abnormal kink-like behavior in PHE is explained by the 1D weak antilocalization correction.[40] (c) Angle-dependent longitudinal resistivity and (d) corresponding APHE in magnetic topological insulator $MnBi_2Te_4$ under different magnetic field ranging from 2 T to 14 T, where the six-fold oscillation is attributed to the orbital magnetic moment.[45] (e) Angle-dependent longitudinal resistivity and (f) corresponding APHE in Weyl semimetal TaP under different magnetic field from 2 T to 14 T, which is attributed to the influence of current jetting effect.[41] (g) Distorted in-plane AMR at the (111) oxide interface between $LaAlO_3$ and $SrTiO_3$ under different gating voltage from −20 V to 50 V, which is explained by the symmetry of crystal structure.[46]

7. Summary and outlook

In this review, we systematically introduce the general mechanisms of PHE, which is originated from the in-plane AMR. There are four main origins for PHE, more specifically the SOC interaction in ferromagnetic materials, time-reversal symmetry breaking process in topological surface states, chiral anomaly in Weyl semimetals, and anisotropic orbital magnetoresistance effect introduced by anisotropic Fermi surface. According to different mechanisms, the sign and the relationship towards magnetic field of PHE amplitude could be effectively distinguished, which can be used to identify the origin of PHE and the underlying properties of these quantum materials. Furthermore, there are many distorted PHE results, providing additional means to detect the buried information such as spins, SOC, symmetry of crystal, and so on. In a spin-polarized system, electronic quantum coherence imposes a correction on PHE, leading to an enhanced slope at different angles. The underlying spin orientation in this system is elucidated, providing a simple method to distinguish spin texture. Moreover, the anisotropy is closely related to the crystal structure (e.g., the quasi-1D structure is likely to exhibit 1D phenomena like Tomonaga–Luttinger liquid effect), and the APHE offers the additional information for anisotropic scattering process as well as the correlated crystal structure. From the analysis of various APHE, there may be a universal principle to connect the anomalous features, directly or indirectly implying the fundamental rule to build an anisotropic system in high-dimensional system. However, the detailed theoretical analysis about APHE is still lacking. More investigations are required to offer new perspectives to understand the movement of electrons in these complex systems.

Acknowledgements

Project supported by the National Natural Science Foundation of China (Grant No. 11904015), the Fundamental Research Funds for the Central Universities (Grant No. YWF-22-K-101), and the National Key R&D Program of China (Grant No. 2018YFE0202700).

References

[1] Hasan M Z and Kane C L 2010 *Rev. Mod. Phys.* **82** 3045
[2] König M, Wiedmann S, Brüne C, Roth A, Buhmann H, Molenkamp L W, Qi X L and Zhang S C 2007 *Science* **318** 766
[3] Noguchi R, Takahashi T, Kuroda K, Ochi M, Shirasawa T, Sakano M, Bareille C, Nakayama M, Watson M D, Yaji K, Harasawa A, Iwasawa

H, Dudin P, Kim T K, Hoesch M, Kandyba V, Giampietri A, Barinov A, Shin S, Arita R, Sasagawa T and Kondo T 2019 *Nature* **566** 518
[4] Tang P, Zhou Q, Xu G and Zhang S C 2016 *Nat. Phys.* **12** 1100
[5] Dufouleur J, Veyrat L, Teichgräber A, Neuhaus S, Nowka C, Hampel S, Cayssol J, Schumann J, Eichler B, Schmidt O G, Büchner B and Giraud R 2013 *Phys. Rev. Lett.* **110** 186806
[6] Cichorek T, Bochenek Ł, Juraszek J, Sharlai Y V and Mikitik G P 2022 *Nat. Commun.* **13** 3868
[7] Chen T, Tomita T, Minami S, Fu M, Koretsune T, Kitatani M, Muhammad I, Nishio-Hamane D, Ishii R, Ishii F, Arita R and Nakatsuji S 2021 *Nat. Commun.* **12** 572
[8] Xu S Y, Belopolski I, Sanchez D S, Neupane M, Chang G, Yaji K, Yuan Z, Zhang C, Kuroda K, Bian G, Guo C, Lu H, Chang T R, Alidoust N, Zheng H, Lee C C, Huang S M, Hsu C H, Jeng H T, Bansil A, Neupert T, Komori F, Kondo T, Shin S, Lin H, Jia S and Hasan M Z 2016 *Phys. Rev. Lett.* **116** 096801
[9] Wu W, Shi Z, Du Y, Wang Y, Qin F, Meng X, Liu B, Ma Y, Yan Z, Ozerov M, Zhang C, Lu H Z, Chu J and Yuan X 2023 *Nat. Mater.* **22** 84
[10] Taychatanapat T, Watanabe K, Taniguchi T and Jarillo-Herrero P 2011 *Nat. Phys.* **7** 621
[11] Das I, Lu X, Herzog-Arbeitman J, Song Z D, Watanabe K, Taniguchi T, Bernevig B A and Efetov D K 2021 *Nat. Phys.* **17** 710
[12] Yoshimi R, Tsukazaki A, Kozuka Y, Falson J, Takahashi K S, Checkelsky J G, Nagaosa N, Kawasaki M and Tokura Y 2015 *Nat. Commun.* **6** 6627
[13] Chong S K, Han K B, Sparks T D and Deshpande V V 2019 *Phys. Rev. Lett.* **123** 036804
[14] Novoselov K S, McCann E, Morozov S V, Fal'ko V I, Katsnelson M I, Zeitler U, Jiang D, Schedin F and Geim A K 2006 *Nat. Phys.* **2** 177
[15] Shamim S, Beugeling W, Böttcher J, Shekhar P, Budewitz A, Leubner P, Lunczer L, Hankiewicz E M, Buhmann H and Molenkamp L W 2020 *Sci. Adv.* **6** eaba4625
[16] Wang P, Tang F, Wang P, Zhu H, Cho C W, Wang J, Du X, Shao Y and Zhang L 2021 *Phys. Rev. B* **103** 155201
[17] Wang H, Liu H, Li Y, Liu Y, Wang J, Liu J, Dai J Y, Wang Y, Li L, Yan J, Mandrus D, Xie X C and Wang J 2018 *Sci. Adv.* **4** eaau5096
[18] Nagaosa N, Sinova J, Onoda S, MacDonald A H and Ong N P 2010 *Rev. Mod. Phys.* **82** 1539
[19] Chang C Z, Zhang J, Feng X, Shen J, Zhang Z, Guo M, Li K, Ou Y, Wei P, Wang L L, Ji Z Q, Feng Y, Ji S, Chen X, Jia J, Dai X, Fang Z, Zhang S C, He K, Wang Y, Lu L, Ma X C and Xue Q K 2013 *Science* **340** 167
[20] Mihály G, Csontos M, Bordács S, Kézsmárki I, Wojtowicz T, Liu X, Jankó B and Furdyna J K 2008 *Phys. Rev. Lett.* **100** 107201
[21] Wang L, Wesselink R J H, Liu Y, Yuan Z, Xia K and Kelly P J 2016 *Phys. Rev. Lett.* **116** 196602
[22] Zhu L, Ralph D C and Buhrman R A 2018 *Phys. Rev. Appl.* **10** 031001
[23] Skinner T D, Olejník K, Cunningham L K, Kurebayashi H, Campion R P, Gallagher B L, Jungwirth T and Ferguson A J 2015 *Nat. Commun.* **6** 6730
[24] Bowen M, Friedland K J, Herfort J, Schönherr H P and Ploog K H 2005 *Phys. Rev. B* **71** 172401
[25] Tang H X, Kawakami R K, Awschalom D D and Roukes M L 2003 *Phys. Rev. Lett.* **90** 107201
[26] Fernández-Pacheco A, De Teresa J M, Orna J, Morellon L, Algarabel P A, Pardo J A, Ibarra M R, Magen C and Snoeck E 2008 *Phys. Rev. B* **78** 212402
[27] Taskin A A, Legg H F, Yang F, Sasaki S, Kanai Y, Matsumoto K, Rosch A and Ando Y 2017 *Nat. Commun.* **8** 1340
[28] Wu B, Pan X C, Wu W, Fei F, Chen B, Liu Q, Bu H, Cao L, Song F and Wang B 2018 *Appl. Phys. Lett.* **113** 011902
[29] Zhou L, Ye B C, Gan H B, Tang J Y, Chen P B, Du Z Z, Tian Y, Deng S Z, Guo G P, Lu H Z, Liu F and He H T 2019 *Phys. Rev. B* **99** 155424
[30] Rakhmilevich D, Wang F, Zhao W, Chan M H W, Moodera J S, Liu C and Chang C Z 2018 *Phys. Rev. B* **98** 094404
[31] Li P, Zhang C, Wen Y, Cheng L, Nichols G, Cory D G, Miao G X and Zhang X X 2019 *Phys. Rev. B* **100** 205128
[32] Nandy S, Sharma G, Taraphder A and Tewari S 2017 *Phys. Rev. Lett.* **119** 176804
[33] Li H, Wang H W, He H, Wang J and Shen S Q 2018 *Phys. Rev. B* **97** 201110
[34] Li P, Zhang C H, Zhang J W, Wen Y and Zhang X X 2018 *Phys. Rev. B* **98** 121108
[35] Zhang N, Zhao G, Li L, Wang P, Xie L, Cheng B, Li H, Lin Z, Xi C, Ke J, Yang M, He J, Sun Z, Wang Z, Zhang Z and Zeng C 2020 *Proc. Natl. Acad. Sci. USA* **117** 11337
[36] Liu Q, Fei F, Chen B, Bo X, Wei B, Zhang S, Zhang M, Xie F, Naveed M, Wan X, Song F and Wang B 2019 *Phys. Rev. B* **99** 155119
[37] Liang D D, Wang Y J, Zhen W L, Yang J, Weng S R, Yan X, Han Y Y, Tong W, Zhu W K, Pi L and Zhang C J 2019 *AIP Adv.* **9** 055015
[38] Kumar N, Guin S N, Felser C and Shekhar C 2018 *Phys. Rev. B* **98** 041103
[39] Yang S Y, Chang K and Parkin S S P 2020 *Phys. Rev. Research* **2** 022029
[40] Zhong J, Yang M, Wang J, Li Y, Liu C, Mu D, Liu Y, Cheng N, Zhuang J, Du Y and Hao W 2023 Submitted
[41] Yang J, Zhen W L, Liang D D, Wang Y J, Yan X, Weng S R, Wang J R, Tong W, Pi L, Zhu W K and Zhang C J 2019 *Phys. Rev. Mater.* **3** 014201
[42] Yang X C, Luo X, Gao J J, Jiang Z Z, Wang W, Wang T Y, Si J G, Xi C Y, Song W H and Sun Y P 2021 *Phys. Rev. B* **104** 155106
[43] Meng J, Xue H, Liu M, Jiang W, Zhang Z, Ling J, He L, Dou R, Xiong C and Nie J 2020 *J. Phys. Condens. Matter* **32** 015702
[44] Huang D, Nakamura H and Takagi H 2021 *Phys. Rev. Research* **3** 013268
[45] Wu M, Tu D, Nie Y, Miao S, Gao W, Han Y, Zhu X, Zhou J, Ning W and Tian M 2022 *Nano Lett.* **22** 73
[46] Rout P K, Agireen I, Maniv E, Goldstein M and Dagan Y 2017 *Phys. Rev. B* **95** 241107
[47] Lozano P M, Cardoso G, Aryal N, Nevola D, Gu G, Tsvelik A, Yin W and Li Q 2022 *Phys. Rev. B* **106** L081124
[48] Galeski S, Legg H F, Wawrzyńczak R, Förster T, Zherlitsyn S, Gorbunov D, Uhlarz M, Lozano P M, Li Q, Gu G D, Felser C, Wosnitza J, Meng T and Gooth J 2022 *Nat. Commun.* **13** 7418
[49] Yang S Y, Wang Y, Ortiz B R, Liu D, Gayles J, Derunova E, Gonzalez-Hernandez R, Šmejkal L, Chen Y, Parkin S S P, Wilson S D, Toberer E S, McQueen T and Ali M N 2020 *Sci. Adv.* **6** eabb6003
[50] Fu H, Wu Y, Zhang R, Sun J, Shan P, Wang P, Zhu Z, Pfeiffer L N, West K W, Liu H, Xie X C and Lin X 2019 *Nat. Commun.* **10** 4351
[51] Sun P, Wei B, Zhang J, Tomczak J M, Strydom A M, Søndergaard M, Iversen B B and Steglich F 2015 *Nat. Commun.* **6** 7475
[52] Alexandrov A S and Zavaritsky V N 2004 *Phys. Rev. Lett.* **93** 217002
[53] Pan Y, Le C, He B, Watzman S J, Yao M, Gooth J, Heremans J P, Sun Y and Felser C 2022 *Nat. Mater.* **21** 203
[54] Ikhlas M, Tomita T, Koretsune T, Suzuki M T, Nishio-Hamane D, Arita R, Otani Y and Nakatsuji S 2017 *Nat. Phys.* **13** 1085
[55] McGuire T and Potter R 1975 *IEEE Trans. Magn.* **11** 1018
[56] Zhao B, Yan X and Pakhomov A B 1997 *J. Appl. Phys.* **81** 5527
[57] Nemoto A, Otani Y, Kim S G, Fukamichi K, Kitakami O and Shimada Y 1999 *Appl. Phys. Lett.* **74** 4026
[58] Cowburn R P, Gray S J, Ferré J, Bland J A C and Miltat J 1995 *J. Appl. Phys.* **78** 7210
[59] Hong K and Giordano N 1995 *Phys. Rev. B* **51** 9855
[60] Ohno H 1998 *Science* **281** 951
[61] Bason Y, Klein L, Wang H Q, Hoffman J, Hong X, Henrich V E and Ahn C H 2007 *J. Appl. Phys.* **101** 09J507
[62] Bason Y, Klein L, Yau J B, Hong X and Ahn C H 2004 *Appl. Phys. Lett.* **84** 2593
[63] Li C Z, Wang L X, Liu H, Wang J, Liao Z M and Yu D P 2015 *Nat. Commun.* **6** 10137
[64] Liang S, Lin J, Kushwaha S, Xing J, Ni N, Cava R J and Ong N P 2018 *Phys. Rev. X* **8** 031002
[65] Collaudin A, Fauqué B, Fuseya Y, Kang W and Behnia K 2015 *Phys. Rev. X* **5** 021022
[66] Ding S, Noël P, Krishnaswamy G K and Gambardella P 2022 *Phys. Rev. Research* **4** L032041
[67] Papadakis S J, De Poortere E P, Shayegan M and Winkler R 2000 *Phys. Rev. Lett.* **84** 5592
[68] Yoshimi R, Tsukazaki A, Kozuka Y, Falson J, Takahashi K S, Checkelsky J G, Nagaosa N, Kawasaki M and Tokura Y 2015 *Nat. Commun.* **6** 6627
[69] Yang M, Liu Y, Zhou W, Liu C, Mu D, Liu Y, Wang J, Hao W, Li J, Zhong J, Du Y and Zhuang J 2022 *ACS Nano* **16** 3036
[70] Zhong J, Yang M, Ye F, Liu C, Wang J, Wang J, Hao W, Zhuang J and Du Y 2022 *Phys. Rev. Appl.* **17** 064017
[71] Cullen J H, Bhalla P, Marcellina E, Hamilton A R and Culcer D 2021 *Phys. Rev. Lett.* **126** 256601